Effect of Turbulence Models in Performance Characterization of a Low Reynolds Number UAV Propeller

Aravind SEENI*

*Corresponding author
International Institute for Aerospace Engineering and Management,
Jain (Deemed-to-be-university), 562112 Bangalore, India,
s.aravind@jainuniversity.ac.in

Abstract: *The advancement of computer technology has given the necessary impetus to perform numerical modelling and simulation in engineering. Turbulence modelling in Computational Fluid Dynamics is characterized by non-physics based modelling and there are several developments in this area that also has contributed to the growing rise in empiricism. Typically, turbulence models are chosen based on expert knowledge and experience. In this paper, the problem of selecting a turbulence closure is addressed for a small Unmanned Aerial Vehicle propeller rotating at a low Reynolds number. Using scientific approaches, verification and validation of performance data against experimental results have been performed for a selected number of turbulence model candidates available in the well-known finite-volume solver Fluent. Modified bivariate plots of performance data error reveal a few numbers of strong candidates of turbulence closures for this problem. After performing a series of checks for consistency, accuracy and computational cost, the two-equation standard k-ω is selected as the preferred model for further propeller simulations.*

Keywords: *turbulence models, UAV propeller, propeller performance, low Reynolds number, numerical accuracy, computational cost*

1. INTRODUCTION

For fluid flow simulations in Computational Fluid Dynamics (CFD), the problem of choosing a turbulence model must be performed based on a compromise between computational calculation accuracy and cost. Simulation of a propeller of an Unmanned Aerial Vehicle (UAV) operating at a low Reynolds number (Re) is an important problem for aerodynamics researchers due to the geometry of the complex three-dimensional propeller, thus providing the need to solve the complex flow boundary layer and the need for a high degree of accuracy for the characterization of the generated aerodynamic propulsion forces. The solution of a turbulent flow problem in CFD is characterized by a degree of empiricism due to the presence of empirically defined coefficients in turbulence modelling. This degree of empiricism potentially induces uncertainty.

Turbulence modelling refers to a set of Partial Differential Equations (PDE) that provide closure to governing Reynolds Averaged Navier-Stokes (RANS) equations. Depending on the type of turbulence model, one can safely classify them based on the number of transport

equations. Hence the models can be referred to as one-equation, two-equation turbulence closures or more.

The following characteristics are the requirements from a CFD simulation employing one of the turbulence models. (a) Computational accuracy – The solution should have an accepted level of accuracy (b) Computational cost – The computational effort should be within reasonably acceptable limits.

It is not accurate to state that two-equation models perform better than one-equation models as in fact simple one-equation models outperform more complex models on both accuracy and cost in certain cases. Moreover, the equations are formulated without any regard to the physics of the problem. The empirical constants in the models are estimated by fitting data to experimental results. The selection of the turbulence model is case specific as there is more than one number of models with implementations potentially overlapping.

The conclusion reached with the selection of the k-ε model for different advance ratios may not be good and may not help the accurate modelling of newly modified propeller shapes, such as a passive slotted propeller [1]. Thus the need for a comprehensive study on the selection of an optimum turbulence model with analysis for different operational conditions is deemed necessary. The study must help to validate the available data through comparison with experimental works of Brandt et al. [2].

This problem is addressed for the case of simulating a propeller operating at Re of approximately 68500. The parameters of interest are the aerodynamic coefficients of thrust and power. The physics of the problem can be narrated. In a freestream corresponding to varied fluid velocities, a propeller operating at a fixed rpm of 3008 produces variable thrust. The torque also varies due to the freestream dependency. The flow separation phenomenon is bound to occur which is not investigated in the current study. The focus is limited to aerodynamic characterization of the selected UAV propeller.

2. METHODOLGY

To test the performance of each of the preselected turbulence closures, a numerical principle validation with known experimental data is performed. The setup proposed in Seeni [3] provides the numerical setup in testing a small-scale UAV propeller called *Applied Precision Composites (APC) 10x7 Slow Flyer*. A full-scale propeller rotating within a cubic computational domain is implemented using the Multiple Reference Frame approach. The rotating speeds considered is 3008 rpm which correspond to a Reynolds number of approximately 68500. The setup includes a rotational reference frame which encloses the 3D propeller and a stationary reference frame surrounding the rotating reference frame. The propeller consists of low *Re* airfoil Eppler 63 near the hub and thin, Clark-Y airfoil sections near the tip. A total of seven turbulence models are tested for fourteen advance ratio conditions. The study consists of a total of 196 simulations.

The commercial solver (Fluent) considered in this study uses the Finite Volume Method to solve the governing equations. The discretization of the flow domain is composed of small 3D fluid control volumes. The seven turbulence models that would be tested within this solver are Spalart-Allmaras, Standard k-ε, realizable k-ε, standard k-ω, SST k-ω, Transition *SST*, Transition k-kl-ω. A no-slip wall condition is imposed on the rotational domain. In order to simulate a range of operational conditions, advance ratios from 0.192 to 0.799 in steps are chosen and the corresponding freestream velocities are applied at the inlet. For certain turbulence models like SST k-ω, the turbulence intensity value is set as per the experimental conditions of [2], [4], [5]. A "coupled" scheme with a Semi-Implicit Method for Pressure-

Linked Equations (SIMPLE) is assumed for the pressure-velocity coupling. A Least-Squares Cell-based algorithm is assigned for gradients. The pressure is assigned with the Standard scheme of interpolation. A second order upwind interpolation scheme is used for Turbulent Dissipation Rate, Turbulent Kinetic Energy and momentum.

2.1 Modelling

2.1.1 Computational domain

The computational domain is designed with two reference frames, stationary and rotational (see Fig. 1). The stationary frame forms a cubic enclosure around the rotational frame with a constant side length of 8D. The rotational reference frame consists of a cylindrical enclosure that surrounds the propeller. The rotational reference frame is designed with a diameter of approximately 1.1D. The velocity inlet is placed at a distance of 4D upstream of the rotational domain. The pressure outlet is equidistantly placed at 4D distance downstream. The implementation of a non-equidistant domain upstream and downstream could potentially allow the wake to vanish downstream however, since only aerodynamic performance computation is our main concern, these dimensions are sufficient. The implementation of a large domain could potentially increase the computational cost, yet a separate study needs to be performed to clarify the accuracy of results due to the domain dependency.
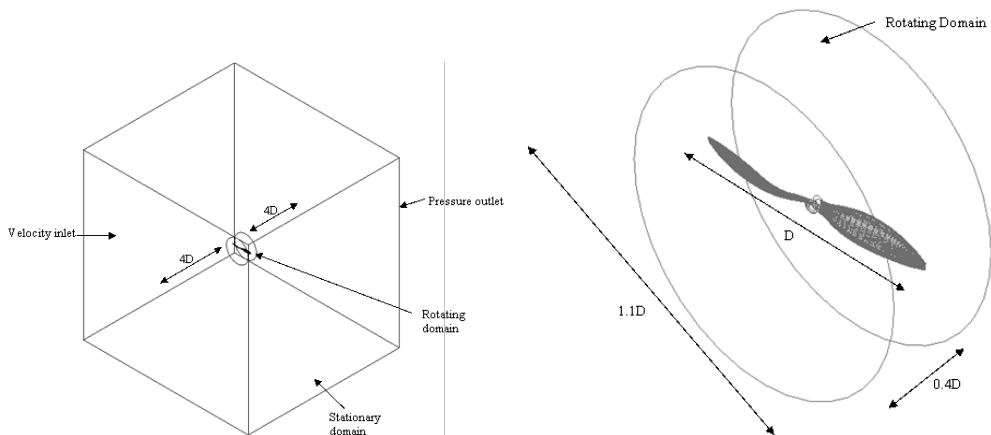

Fig. 1 – Computational domain (top); rotational domain with propeller and cylindrical enclosure (bottom)

2.1.2 Mesh

The domain is discretized into smaller elements, each forming small three-dimensional fluid control volumes. An unstructured mesh design is adopted for both the stationary and the rotational domain. The reason for such an approach can be attributed to geometric complexity. While the use of structured mesh can be favored for its refined topology, the use of the unstructured mesh does not impact the accuracy of computational results [6].

The wall y+ of the mesh partly specifies the requirements for modelling the mesh for each turbulence model. Depending on the turbulence model requirements, the meshes are employed with suitable y+ at the wall. For instance, the transition models require y+ of less than 1. Hence meshes with different wall y+ are used in this study. The k-ω model with standard wall function and variant realizable k-ω with scalable wall function as considered requires a mesh, in principle, with wall y+~1 as in this case of flows at low *Re*. The transition models, k-kl-ω and transition SST also require a similar adoption to capture laminar to turbulent transition. The SST k-ω model is implemented as an enhanced wall treatment. This employs the two-

layer model, the law of the wall or as a blending function of the two. Therefore, the requirement of y+<1 is not strictly binding. The SST k-ω model is as accurate as the k-ε model when y+ above 11 is implemented. In such a case, a logarithmic wall function will be used to calculate the shear stress at the wall. In case of further refinements, the transition to a linear wall function occurs in which more accurate results are computed. The above points are also applicable for the standard k-ω model.

2.1.3 Turbulence modelling

For an incompressible flow, the Navier-Stokes equations can be written as follows:

$$\frac{\partial y}{\partial X_i}(\rho U_i) = 0 \tag{1}$$

$$\frac{\partial y}{\partial X_j}(\rho U_j U_i) = \frac{-\partial P}{\partial X_i} + \frac{\partial}{\partial X_j}(t_{ij} + \rho \tau_{ij}) \tag{2}$$

In the two-equation standard k-ε model, two differential equations are solved, one for turbulence energy (k) and another for dissipation rate of turbulence energy (ε). Traditionally, it is the chosen model for practical engineering flow applications. The two-equation standard k-ε model is given by the following equations [7]:

$$\frac{D\epsilon}{Dt} = \frac{1}{\rho}\frac{\partial}{\partial x_j}\left[\left(\frac{\mu_t}{\sigma_c}+\mu\right)\frac{\partial \epsilon}{\partial x_j}\right] + C_1 \frac{\epsilon}{k}\frac{\mu_t}{\rho}\frac{\partial U_i}{\partial x_j}\left(\frac{\partial U_i}{\partial x_j}+\frac{\partial U_i}{\partial x_i}\right) - \frac{C_2 \varepsilon^2}{k} - \frac{2v\mu_t}{\rho}\left(\frac{\partial^2 U_i}{\partial x_j \partial x_i}\right)^2 \tag{3}$$

$$\frac{Dk}{Dt} = \frac{1}{\rho}\frac{\partial}{\partial x_j}\left[\left(\frac{\mu_t}{\sigma_k}+\mu\right)\frac{\partial k}{\partial x_j}\right] + \frac{\mu_t}{\rho}\frac{\partial U_i}{\partial x_j}\left(\frac{\partial U_i}{\partial x_j}+\frac{\partial U_i}{\partial x_i}\right) - 2v\left(\frac{\partial k^{1/2}}{\partial x_j}\right)^2 - \varepsilon \tag{4}$$

The realizable k-ε model is given by the following equations [8]:

$$\frac{\partial}{\partial t}(\rho k) + \frac{\partial}{\partial x_j}(\rho k u_j) = \frac{\partial}{\partial x_j}\left[\left(\mu+\frac{\mu_t}{\sigma_k}\right)\frac{\partial k}{\partial x_j}\right] + P_k + P_b - \rho\epsilon - Y_M + S_k \frac{\partial}{\partial t}(\rho\epsilon) + \frac{\partial}{\partial x_j}(\rho\epsilon u_j)$$
$$= \frac{\partial}{\partial x_j}\left[\left(\mu+\frac{\mu_t}{\sigma_\epsilon}\right)\frac{\partial \epsilon}{\partial x_j}\right] + \rho C_1 S\epsilon - \rho C_2 \frac{\epsilon^2}{k+\sqrt{v\epsilon}} + C_{1\epsilon}\frac{\epsilon}{k}C_{3\epsilon}P_b + S_\epsilon \tag{5}$$

$$\frac{\partial}{\partial t}(\rho k) + \frac{\partial}{\partial x_j}(\rho k u_j) = \frac{\partial}{\partial x_j}\left[\left(\mu+\frac{\mu_t}{\sigma_k}\right)\frac{\partial k}{\partial x_j}\right] + P_k + P_b - \rho\epsilon - Y_M + S_k \tag{6}$$

$$\frac{\partial}{\partial t}(\rho\epsilon) + \frac{\partial}{\partial x_j}(\rho\epsilon u_j) = \frac{\partial}{\partial x_j}\left[\left(\mu+\frac{\mu_t}{\sigma_\epsilon}\right)\frac{\partial \epsilon}{\partial x_j}\right] + \rho C_1 S\epsilon - \rho C_2 \frac{\epsilon^2}{k+\sqrt{v\epsilon}} + C_{1\epsilon}\frac{\epsilon}{k}C_{3\epsilon}P_b + S_\epsilon \tag{7}$$

In the two-equation standard k-ω model, two equations are solved, one for turbulence kinetic energy (k) and another for specific dissipation rate (ω). The model is given by the following equations [9]:

$$\frac{\partial(\rho k)}{\partial t} + \frac{\partial(\rho u_j k)}{\partial x_j} = \rho \tau_{ij}\frac{\partial u_i}{\partial x_j} - \beta^* \rho k\omega + \frac{\partial}{\partial x_j}\left[\left(\mu+\sigma^*\frac{\rho k}{\omega}\right)\frac{\partial k}{\partial x_j}\right] \tag{8}$$

$$\frac{\partial(\rho\omega)}{\partial t} + \frac{\partial(\rho u_j\omega)}{\partial x_j} = \alpha\frac{\omega}{k}\rho\tau_{ij}\frac{\partial u_i}{\partial x_j} - \beta\rho\omega^2 + \sigma_d\frac{\rho}{\omega}\frac{\partial k}{\partial x_j}\frac{\partial\omega}{\partial x_j} + \frac{\partial}{\partial x_j}\left[\left(\mu+\sigma\frac{\rho k}{\omega}\right)\frac{\partial\omega}{\partial x_j}\right] \tag{9}$$

The Menter's Shear Stress Transport (SST) k-ω model is a modification of the standard k-ω model. The two equations governing the transport model can be expressed as follows [10]:

$$\frac{\partial(\rho k)}{\partial t} + \frac{\partial(\rho u_j k)}{\partial x_j} = \tau_{ij}\frac{\partial u_i}{\partial x_j} - \beta^* \rho \omega k + \frac{\partial}{\partial x_j}\left[(\mu + \sigma_k \mu_t)\frac{\partial k}{\partial x_j}\right] \tag{10}$$

$$\frac{\partial(\rho \omega)}{\partial t} + \frac{\partial(\rho u_j \omega)}{\partial x_j} = \frac{\gamma}{v_t}\tau_{ij}\frac{\partial u_i}{\partial x_j} - \beta \rho \omega^2 + \frac{\partial}{\partial x_j}\left[(\mu + \sigma_\omega \mu_t)\frac{\partial \omega}{\partial x_j}\right] + 2(1 - F_1)\frac{\rho \sigma_{w2}}{\omega}\frac{\partial k}{\partial x_j}\frac{\partial \omega}{\partial x_j} \tag{11}$$

The equations for all the models are described in detail in ANSYS Fluent theory guide [11].

3. RESULTS AND DISCUSSIONS

3.1 Verification and Validation

3.1.1 Validation

In the validation process, I compare CFD results with experimentally obtained data, herein referred to as Experimental Fluid Dynamics (EFD). The difference between the EFD and CFD data can be termed as the Error (E). The error can be expressed as percentage and can be calculated using the following definition: $E = \frac{EFD - CFD}{EFD} \times 100$. The numerically computed results along with the error are made available in tabulated form.

Table 1 lists the thrust coefficient and

Table 2 lists the power coefficient results. The tables suggest that thrust coefficient and power coefficient can be computed within reasonable margins. The global error was found to be less than 5%. The global error for K_T is at -1.2%, K_P at -2.44%. It is desired to use the power coefficient as a performance coefficient rather than the torque since torque is a miniscule quantity and cannot be easily interpreted numerically.

Therefore, the power coefficient which is estimated from the torque computations is used and presented. The tables further suggest that the thrust and power coefficients have been found to be computed within reasonable margins by all turbulence models for the 14 cases considered.

The EFD results also present an uncertainty as for all experimental results exhibit errors. The level of uncertainty for EFD results considered here is zero percent as Refs. [2], [4], [12] do not provide that information.

It is vital that this uncertainty be as low as possible or within acceptable range for performing any meaningful discussion from the presented results [13].

3.1.2 Verification

The numerical verification of the results is performed through Grid Resolution Method. It is an important step to find the optimal mesh size that is sufficient to provide grid independent solutions. The method involves increasing the mesh size, such that the performance parameters exhibit negligible variations until no further refinement is necessary.

Five meshes, M1 to M5 of increasing grid resolutions, as listed in Table 3, are used to perform this study. The Grid Resolution Method utilizes the smallest error difference in result with changes in grid resolution.

A mid-advance ratio condition of 0.486 is chosen to perform this test. This mid-advance ratio condition is chosen due to small error generation compared to other very low or high advance ratios where the error generated is relatively large. The condition 0.486 advance ratio generated the least error among all advance ratios.

Table 1 – Experimental and numerical results comparison and validation for thrust coefficient

Case	*J*	Type	*S-A*	*Std. k-ε*	*Real. k-ε*	*Std. k-ω*	*SST k-ω*	*Trans. SST*	*Trans. k-kl-ω*	Mean
1	0.192	EFD	0.1257							-
		CFD	0.1092	0.1110	0.1062	0.110	0.110	0.110	0.109	0.1095
		E	-13.12%	-11.69%	-15.54%	-12.16%	-12.50%	-12.35%	-13.12%	-12.93%
2	0.236	EFD	0.1181							-
		CFD	0.1057	0.1071	0.1070	0.1065	0.1064	0.1066	0.1067	0.1066
		E	-10.48%	-9.28%	-9.36%	-9.80%	-9.93%	-9.75%	-9.66%	-9.75%
3	0.282	EFD	0.1109							-
		CFD	0.1009	0.1030	0.1019	0.1021	0.1024	0.1025	0.1025	0.1022
		E	-9.05%	-7.13%	-8.12%	-7.97%	-7.70%	-7.55%	-7.59%	-7.87%
4	0.334	EFD	0.1027							-
		CFD	0.0951	0.0973	0.0961	0.0960	0.0959	0.0962	0.0968	0.0962
		E	-7.40%	-5.21%	-6.45%	-6.55%	-6.66%	-6.31%	-5.74%	-6.33%
5	0.383	EFD	0.095							-
		CFD	0.0885	0.0905	0.0901	0.0900	0.0897	0.0896	0.0897	0.0897
		E	-6.80%	-4.70%	-5.12%	-5.26%	-5.55%	-5.64%	-5.62%	-5.53%
6	0.432	EFD	0.0865							-
		CFD	0.0815	0.0834	0.0829	0.0824	0.0824	0.0825	0.0826	0.0825
		E	-5.81%	-3.58%	-4.19%	-4.72%	-4.72%	-4.62%	-4.57%	-4.60%
7	0.486	EFD	0.0766							-
		CFD	0.0731	0.0742	0.0744	0.0739	0.0741	0.0742	0.0740	0.0740
		E	-4.56%	-3.19%	-2.86%	-3.50%	-3.25%	-3.19%	-3.38%	-3.42%
8	0.527	EFD	0.0692							-
		CFD	0.0657	0.0674	0.0674	0.0670	0.0670	0.0671	0.0665	0.0669
		E	-5.09%	-2.65%	-2.66%	-3.14%	-3.25%	-3.09%	-3.89%	-3.39%
9	0.573	EFD	0.0607							-
		CFD	0.0573	0.0591	0.0586	0.0584	0.0583	0.0583	0.0582	0.0583
		E	-5.64%	-2.56%	-3.53%	-3.71%	-4.01%	-3.94%	-4.10%	-3.93%
10	0.628	EFD	0.0493							-
		CFD	0.0464	0.0478	0.0479	0.0480	0.0475	0.0475	0.0478	0.0476
		E	-5.86%	-2.96%	-2.77%	-2.55%	-3.75%	-3.66%	-3.02%	-3.51%
11	0.659	EFD	0.0426							-
		CFD	0.0400	0.0418	0.0416	0.0416	0.0413	0.0413	0.0410	0.0412
		E	-6.08%	-1.82%	-2.43%	-2.33%	-3.00%	-3.08%	-3.86%	-3.23%
12		EFD	0.029							-

Case	J	Type	S-A	Std. k-ε	Real. k-ε	Std. k-ω	SST k-ω	Trans. SST	Trans. k-kl-ω	Mean
	0.717	CFD	0.0277	0.0291	0.0295	0.0295	0.0284	0.0289	0.0288	0.0289
		E	-4.36%	0.41%	1.82%	1.64%	-1.98%	-0.32%	-0.82%	-0.52%
13	0.773	EFD	0.0143							-
		CFD	0.0153	0.0170	0.0163	0.0171	0.0161	0.0168	0.0158	0.0164
		E	6.86%	19.22%	14.32%	19.32%	12.55%	17.65%	10.83%	14.39%
14	0.799	EFD	0.0078							-
		CFD	0.0092	0.0109	0.0110	0.0108	0.0101	0.0108	0.0102	0.0104
		E	17.62%	39.89%	41.57%	37.92%	29.91%	38.39%	31.19%	33.78%
Mean			-4.27%	0.34%	-0.38%	-0.20%	-1.70%	-0.53%	-1.67%	**-1.20%**

Table 2 – Experimental and numerical results comparison and validation for power coefficient

Case	J	Type	S-A	Std. k-ε	Real. k-ε	Std. k-ω	SST k-ω	Trans. SST	Trans. k-kl-ω	Mean
1	0.192	EFD	0.6810							-
		CFD	0.6239	0.6184	0.6171	0.614	0.610	0.609	0.603	0.6138
		E	-8.39%	-9.19%	-9.38%	-9.78%	-10.41%	-10.51%	-11.46%	-9.87%
2	0.236	EFD	0.662							-
		CFD	0.6217	0.6107	0.6099	0.6085	0.6051	0.6045	0.5822	0.6061
		E	-6.09%	-7.74%	-7.88%	-8.09%	-8.60%	-8.69%	-12.06%	-8.45%
3	0.282	EFD	0.646							-
		CFD	0.6136	0.6039	0.5951	0.6014	0.6019	0.6010	0.5952	0.6017
		E	-5.01%	-6.52%	-7.88%	-6.90%	-6.82%	-6.96%	-7.87%	-6.85%
4	0.334	EFD	0.629							-
		CFD	0.6020	0.5912	0.5812	0.5888	0.5873	0.5872	0.5822	0.5886
		E	-4.29%	-6.01%	-7.60%	-6.39%	-6.63%	-6.65%	-7.45%	-6.43%
5	0.383	EFD	0.61							-
		CFD	0.5863	0.5713	0.5656	0.5762	0.5728	0.5708	0.5609	0.5720
		E	-3.88%	-6.34%	-7.28%	-5.54%	-6.10%	-6.43%	-8.05%	-6.23%
6	0.432	EFD	0.586							-
		CFD	0.5660	0.5500	0.5425	0.5529	0.5512	0.5504	0.5401	0.5505
		E	-3.42%	-6.15%	-7.42%	-5.64%	-5.94%	-6.07%	-7.84%	-6.07%
7	0.486	EFD	0.553							-
		CFD	0.5412	0.5257	0.5175	0.5263	0.5267	0.5257	0.5142	0.5253
		E	-2.13%	-4.94%	-6.42%	-4.82%	-4.76%	-4.94%	-7.01%	-5.00%
8	0.527	EFD	0.526							-
		CFD	0.5146	0.4975	0.5175	0.5041	0.5020	0.5012	0.4863	0.5033
		E	-2.16%	-5.42%	-1.62%	-4.16%	-4.56%	-4.72%	-7.54%	-4.31%
9	0.573	EFD	0.492							-
		CFD	0.4849	0.4680	0.4629	0.4718	0.4699	0.4677	0.4578	0.4690
		E	-1.44%	-4.88%	-5.92%	-4.10%	-4.50%	-4.93%	-6.96%	-4.68%
10	0.628	EFD	0.444							-

		CFD	0.4430	0.4257	0.4236	0.4329	0.4285	0.4273	0.4202	0.4287
		E	-0.22%	-4.11%	-4.60%	-2.51%	-3.50%	-3.76%	-5.35%	-3.44%

Case	J	Type	*S-A*	*Std. k-ε*	*Real. k-ε*	*Std. k-ω*	*SST k-ω*	*Trans. SST*	*Trans. k-kl-ω*	Mean
11	0.659	EFD	0.417							-
		CFD	0.3881	0.4021	0.3991	0.4059	0.4044	0.4016	0.3933	0.3992
		E	-6.93%	-3.57%	-4.28%	-2.66%	-3.03%	-3.68%	-5.69%	-4.26%
12	0.717	EFD	0.355							-
		CFD	0.3638	0.3512	0.3487	0.3540	0.3496	0.3483	0.3455	0.3516
		E	2.48%	-1.07%	-1.76%	-0.27%	-1.51%	-1.89%	-2.68%	-0.96%
13	0.773	EFD	0.283							-
		CFD	0.3101	0.2982	0.4765	0.3003	0.2954	0.2960	0.2911	0.3239
		E	9.59%	5.35%	68.37%	6.10%	4.38%	4.60%	2.86%	14.46%
14	0.799	EFD	0.252							-
		CFD	0.2839	0.2730	0.4417	0.2740	0.2704	0.2706	0.2654	0.2970
		E	12.64%	8.35%	75.29%	8.74%	7.29%	7.39%	5.32%	17.86%
Mean			-1.37%	-3.73%	5.12%	-3.29%	-3.91%	-4.09%	-5.84%	**-2.44%**

Table 3 – Mesh refinements considered for grid independence study

Grid	Refinement level	Total nodes	Total elements
M1	Coarsest	41927	199380
M2	Coarse	165545	789650
M3	Medium	242877	1141968
M4	Mid-fine	292342	1374053
M5	Fine	798178	3763486

Table 4 – Grid Independence Test for thrust coefficient, power coefficient for case 7, *J*=0.486

Parameter	Type	Error [%]				
		Coarsest	Coarse	Medium	Mid-fine	Fine
K_T	EFD	0.0766				
	CFD	0.0793	0.0718	0.0670	0.0678	0.0625
	E	3.48%	-6.21%	-12.59%	-11.47%	-18.42%
$10K_P$	EFD	0.5530				
	CFD	0.6132	0.5655	0.5346	0.5440	0.5033
	E	10.88%	2.26%	-3.33%	-1.63%	-9.00%

Contrary to the notion that the finest grid provides better results, Table 4 suggests that the smallest error in the thrust coefficient is present in the coarsest grid whereas the smallest error in power coefficient is present in the mid-fine grid.

The power coefficient results are overlooked since by definition it is deduced from torque which is a miniscule quantity.

The thrust coefficient which is derived from the thrust force is considered to be a better quantity. Thus coarse mesh grid is most suitable for this study.

The results purportedly show that increasing the mesh resolution reduces the accuracy of results, as is evident in Table 4.

3.2 Comparison of results

The thrust coefficient is predicted remarkably well by all the turbulence models with a global error of only -1.2%. While the power coefficient also is predicted reasonably well (with acceptable error of -2.44%), it is resorted to discuss one parameter with particular emphasis to capture the influence of varied turbulence models. Hence, it would be worthwhile to examine the results of the thrust coefficient in greater detail. The thrust coefficient is effectively a function of the thrust force generated in the axial direction. Here, I examine the results of the thrust coefficient for each advance ratio condition in order to perform the ultimate conclusive step of determining the optimum turbulence model.

3.2.1 Thrust coefficient

Although the global error for the thrust coefficient was found to be considerably low, that does not mean that the turbulence models were able to accurately replicate the experimental data within reasonable limits. The results suggest that the turbulence models were not able to achieve a high accuracy for several advance ratio conditions. Notably, at low advance ratios of 0.192, the error was found to be greater than 10% for all models. At high advance ratios, 0.773 and 0.799, the errors were too large. In spite of these facts, it can be stated that the turbulence models were able to find reasonably accurate results within the error bound of less than 10% for advance ratio band between 0.236 and 0.717. Thus it can be inferred that the chosen turbulence models are applicable for this problem. Furthermore, for advance ratios from 0.192 to 0.659, the turbulence models provide underestimated results. For advance ratio of 0.717, the models provide a mix of under and overestimated results, but well within acceptable error range. Beyond this advance ratio, the results are overestimated. As stated earlier, most results are found to be within an acceptable error range while a few for isolated conditions produce large errors. It was further deduced that the results for any advance ratio condition, do not vary significantly among themselves. All models produce more or less identical results for given advance ratio. The thrust coefficient was computed by all turbulence models within a global average of less than 5% (in absolute terms) for all advance ratio conditions. Among the seven RANS closures selected, the standard k-ω was able to provide an error average of just 0.20%. The average was calculated by including the low and high advance ratios with higher errors stated above. If the higher errors are neglected, the error percentage will be still lower. Nevertheless, it is necessary to choose one particular optimum model than provides the best performance computation.

3.2.2 Identifying optimum turbulence model

The earlier sections provided validated results and quantified errors through comparison of CFD and EFD data. It was generally observed that the errors were high at low advance ratios which gradually reduces up to an advance ratio of 0.717 and then begins to increase for higher advance ratios. The next step is to find a solution to check for consistency within the data. To perform this, a modified Youden [14] plot method will be adopted. I will now use the technique (with some limited modifications) to find a solution for this aerodynamic propeller case considered in this study. First, I declare that the uncertainty in experimental data is unknown and therefore it will not be included in our plots.

Secondly, the errors for most advance ratio conditions with the exemption of case 12, 13 and 14 produce underestimated results compared to experiment and therefore the scatter plots produce data lying only in the third quadrant unlike the homogeneity of data scatter in several quadrants observed by Terziev et al. [15].

The modified Youden [14] plot technique, involves plotting the error for each parameter in an *x-y* plane. The errors are plotted as coordinates *[x,y]=[E₁,E₂]* where the subscripts indicate the case study number. Four case studies are generally considered for each plot and therefore points with *[x,y]=[E₃,E₄]* are also plotted in the same plot, with different markers. Now, straight lines are constructed that represents the median *x* and *y* values. This step allows establishing bias or lack thereof.

Then, a 45 degree diagonal is drawn using the intersection of median values. This step is performed to establish the hierarchy of points close to the diagonal. Points close to the diagonal perform better in consistency and perform similarly or systematically in all four case studies. A few modifications are considered in this study before I progress with drawing the plots. The step of drawing median lines is neglected due to the reason that error points in most cases from 1 to 11 are mostly negative.

The 45 degree diagonal is drawn using the origin as vertex since experimental data uncertainty is unknown for all 14 cases. I thus assume that the experimental uncertainty is practically zero and have been reproduced with higher accuracy. Fig. 2, 5, 6 and 7 are drawn using errors estimated for thrust coefficient for cases 1-4, 5-8, 9-12 and 13-14 respectively.

A greater offset from the diagonal drawn on these figures indicate erratic behaviour of turbulence models. Points close to the diagonal reveal greater consistency. Fig. 2 plot is inconclusive in finding the best turbulence model as the scatter of data is relatively close, lies within a fixed proximity and case specific. For certain cases, the transition SST and SST k-ω points lie close to diagonal indicating better consistency. Yet, the plot is inconclusive in determining optimum closure for the cases considered due to its case specific nature. The same can be said about the plots in Figs. 5, 6 and 7. In the above plots, only the thrust coefficient is taken into account. The inconclusive nature of the earlier plots allows us to construct more plots considering the power coefficient plotted in x-axis and the thrust coefficient plotted in y-axis. Two cases will be considered for each plot and the cases considered are 1 and 2, 3 and 4, 5 and 6. The plotted results are shown in Figs. 8, 9 and 10.
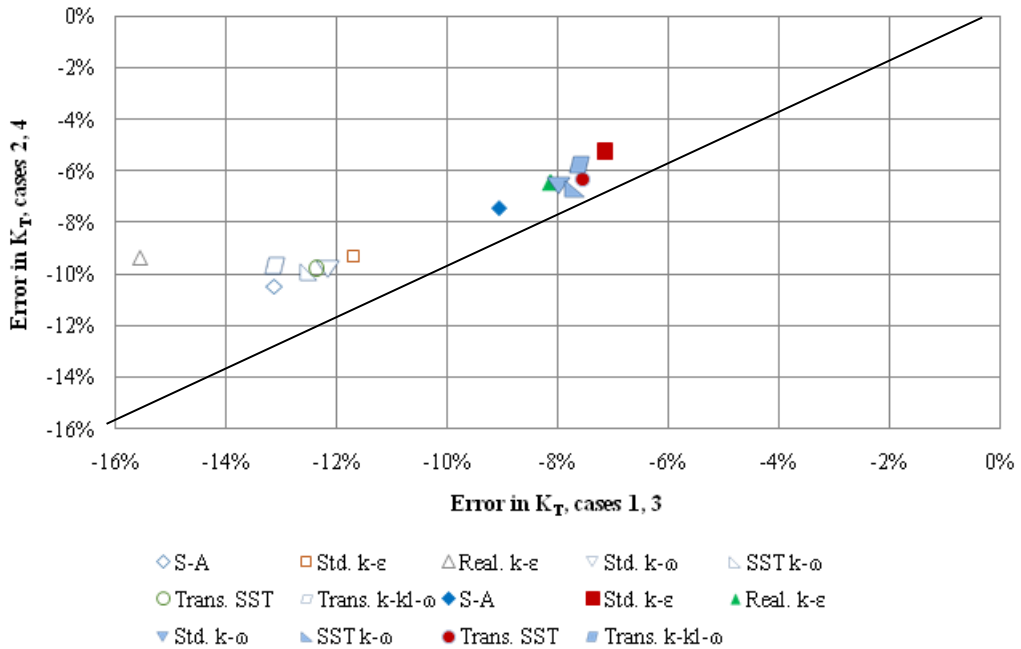

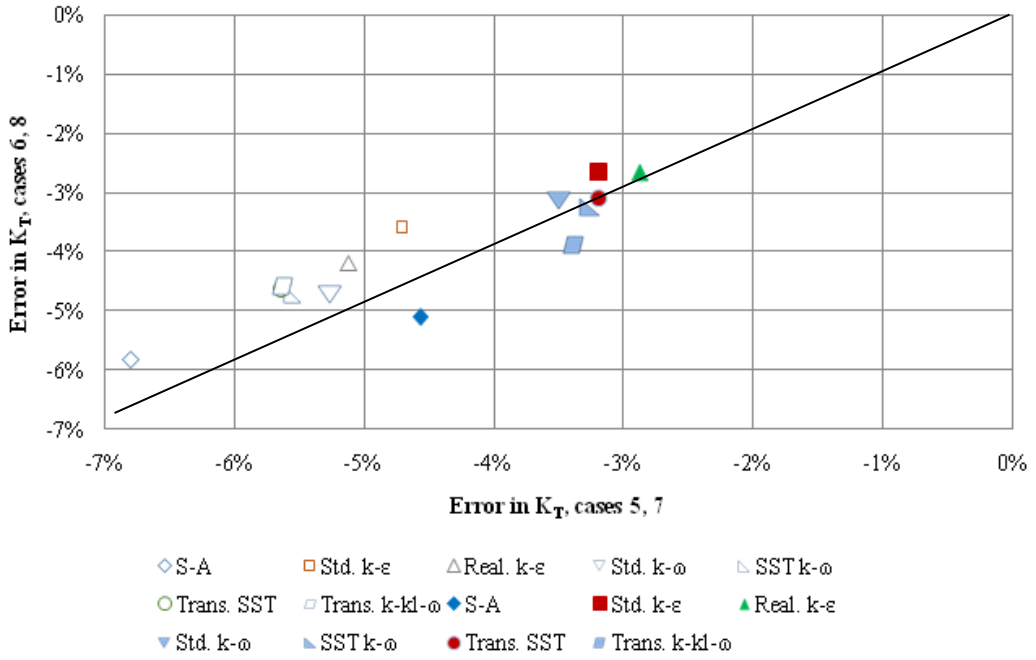Fig. 2 – Bivariate error plot of thrust coefficient, cases 1-4

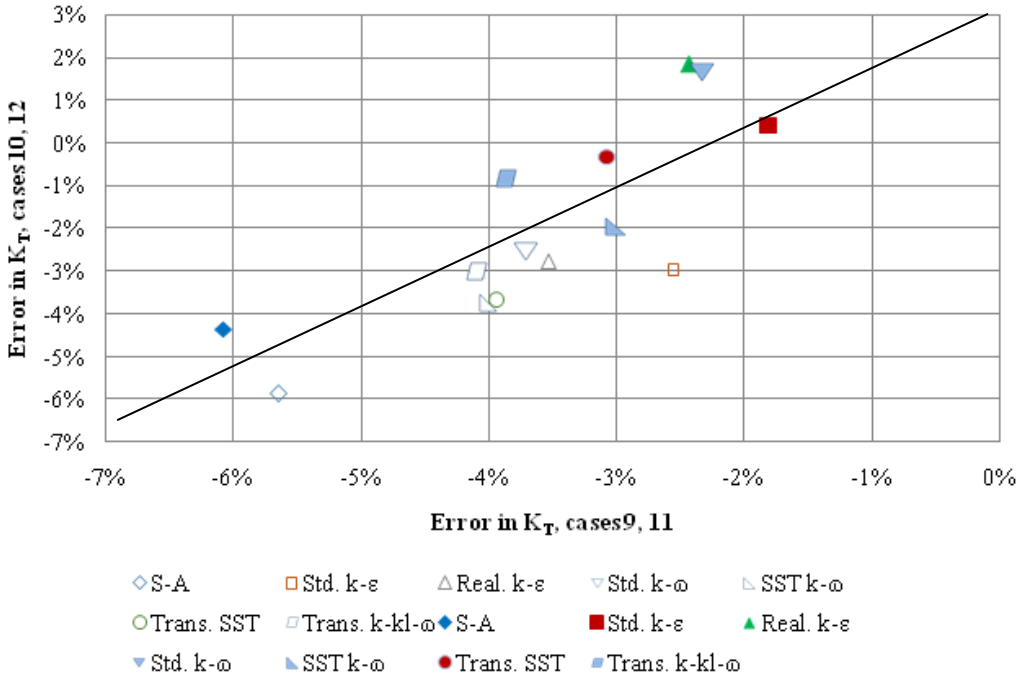Fig. 3 – Bivariate error plot of thrust coefficient, cases 5-8

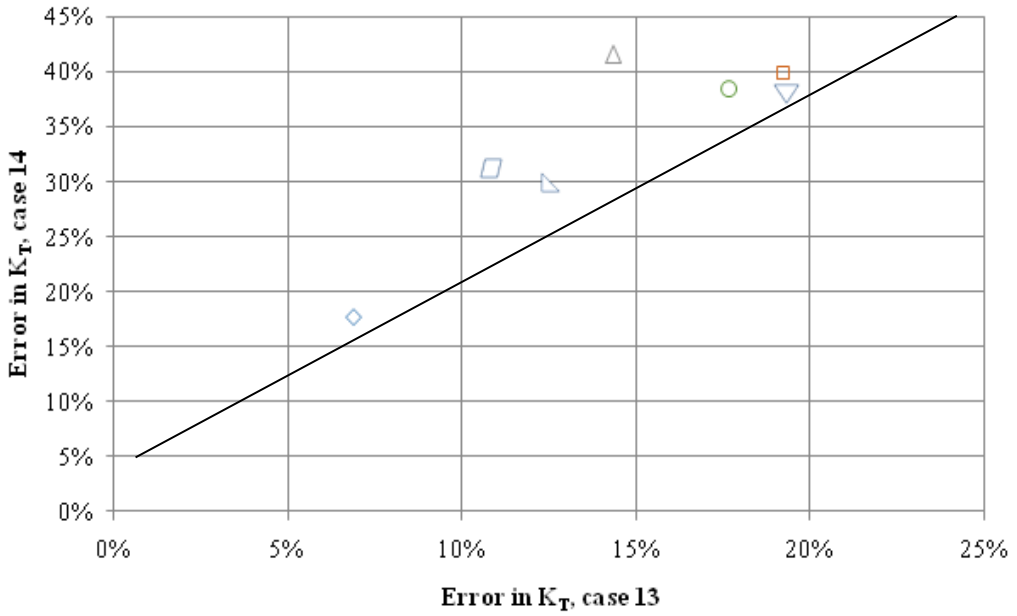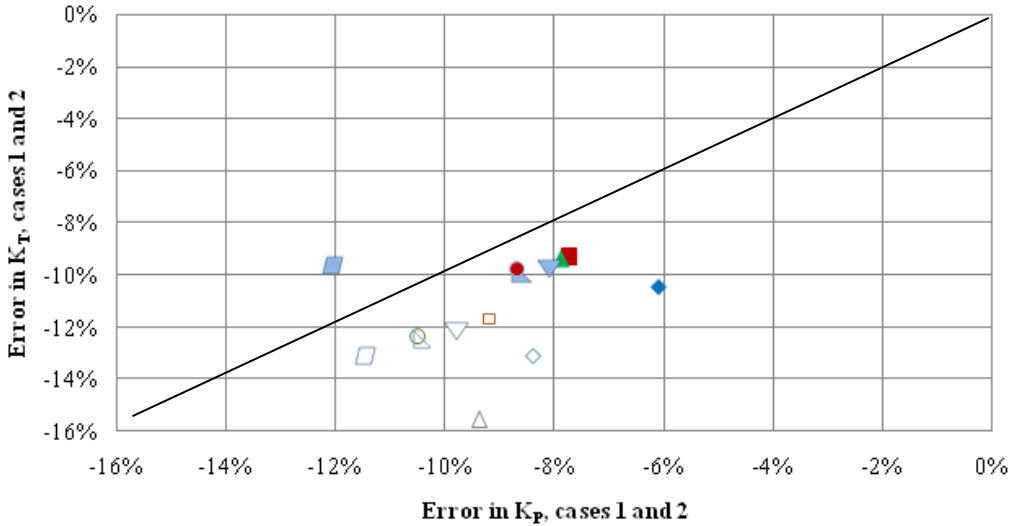Fig. 4 – Bivariate error plot of thrust coefficient, cases 9-12

Fig. 5 – Bivariate error plot of thrust coefficient, cases 13-14

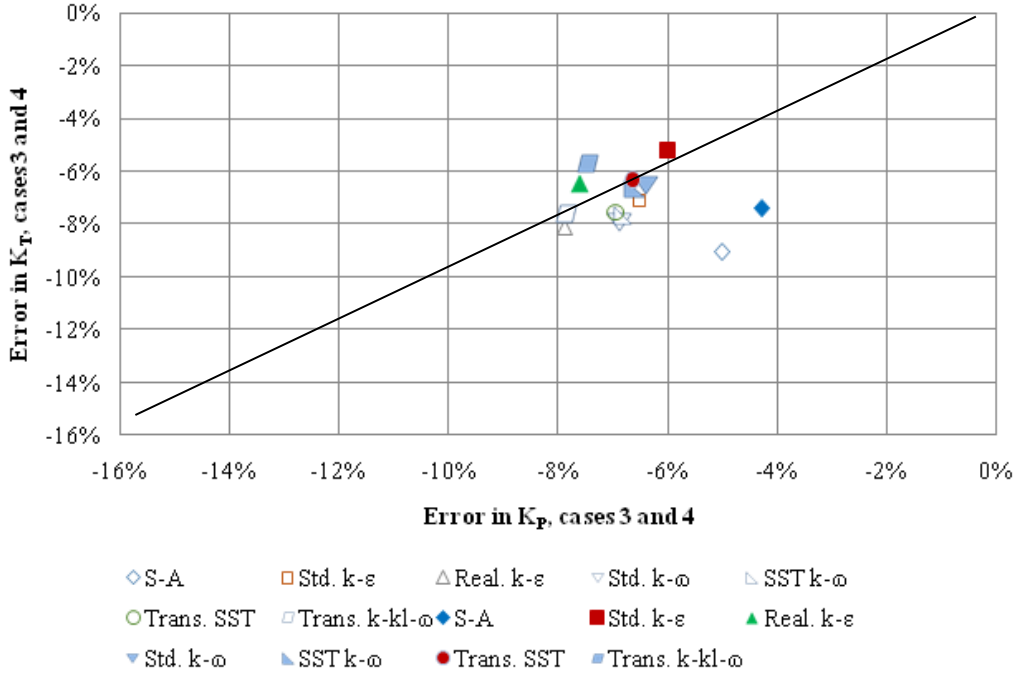Fig. 6 – Bivariate error plot of power coefficient vs. thrust coefficient, cases 1 and 2

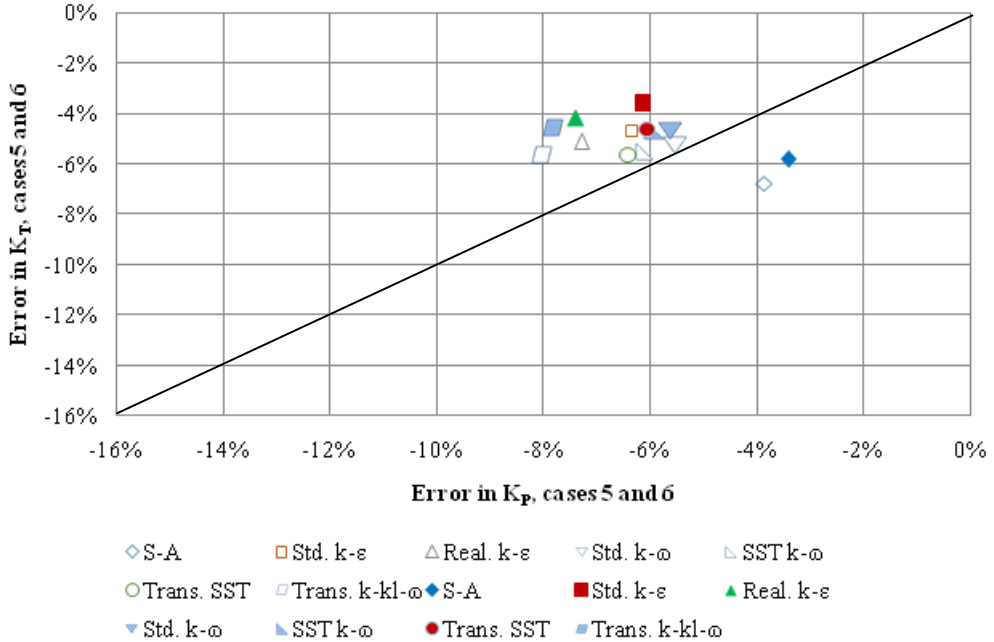Fig. 7 – Bivariate error plot of power coefficient vs. thrust coefficient, cases 3 and 4

Fig. 8 – Bivariate error plot of power coefficient vs. thrust coefficient, cases 5 and 6

The analysis of these plots is more revealing that in earlier cases. It can be observed in Fig. 6 that most points lie below the diagonal. In Fig. 7 with advancement in advance ratio, the points move in closer proximity to the diagonal with data points split between upper and lower part of the diagonal. The same trend follows for even higher advance ratios in Fig. 8 where most

points lie above the diagonal. Overall, the transition SST, standard k-ω and SST k-ω are found to have better consistency over other turbulence models in the three plots. This can be attributed to the smaller distance between the points to the diagonal. All three also lie almost equidistant from the origin indicating less bias. The distance to the diagonal serves as an important metric in the present study and serves as an indication to pick the robust turbulence model. The smallest distance from the points to the diagonal will indicate good consistency. As discussed previously, it is essential that the points be in a smaller distance from the diagonal indicating the robustness of the turbulence model to be particularly applicable for this problem. The robustness here portrays applicability for all cases or different advance ratios. The distance to the diagonal should be small for different advance ratios. Larger distance as exhibited by the Spalart-Allmaras is unreliable and erratic in principle. The above consideration requires analysis of bivariate plots considering both power and thrust coefficient. As is evident in Fig. 8 the realizable k-ε performed marginally worse compared to other models. The Spalart-Allmaras also performed with highly/ extremely inconsistent behaviour (see Figs. 8 and 9). Also, the standard k-ε did not seem to be very accurate, as in the case with the k-kl-ω Transition (see Fig. 8).

3.2.3 Computational cost requirements

Fig. 9 – Computational expense comparison for case 1. Model average marked as dotted line.

Fig. 9 compares the computational cost of all seven turbulence models with inviscid and laminar flow conditions for the case of 0.192 advance ratio. The inviscid model followed by the laminar model took the smallest computational effort. As is evident in the figure, the one-equation Spalart-Allmaras model took the smallest amount of computational effort among the turbulence models considered. This is followed by the two equation k-ε closures. Among the k-ε models, the realizable k-ε model employed with scalable wall functions required slightly additional effort compared to standard wall function. The standard k-ω and SST k-ω followed close in the computational effort taken. The four-equation transition SST had reduced computational cost compared to the three equation k-kl-ω model. Yet, the cost incurred by

both these models is above average. Nevertheless, the trend is clear that improvement in model complexity due to additional equations as well as wall function have a distinct impact on the computational cost. For our low Reynolds propeller problem, the transition SST model provides accurate results, albeit at a higher computational cost. The standard k-ω has the advantage of both as a cost-effective model without impeding the accuracy. The SST k-ω model produces accurate results, only at a slightly higher expense in computational cost compared to the standard k-ω model.

4. CONCLUSIONS

This study was performed with the objective of selecting turbulence models for the problem of simulating a propeller operating at low *Re*. Out of many available turbulence models coded in the RANS solver Fluent, seven eddy-viscosity turbulent models were chosen as candidates for performance testing. The problem concerned is the simulation of a rotating small scale propeller operating at a Reynolds number of 68500. The models were tested on as they show the best performance in terms of aerodynamic characterization accuracy and computational cost. Thrust and torque coefficients were obtained. The solutions derived from the models were validated against available experimental data. In the process errors were measured and made available for all fourteen different advance ratios and freestream velocity conditions. The results show that all turbulence models managed to provide results within acceptable level of accuracy and within reasonable error margins. The selection of the optimum model was performed through bivariate analysis. The selection of turbulence models was performed through consistency and accuracy analysis. The solutions revealed three turbulence models, transition SST, standard k-ω and SST k-ω as best fit to this problem. The turbulence models were further analyzed on the amount of computational effort required to complete a simulation. Overall the results revealed that the standard k-ω model exhibited the best performance when a trade-off on accuracy and computational cost was made.

REFERENCES

[1] H. A. Kutty, P. Rajendran, and A. Mule, Performance analysis of small scale UAV propeller with slotted design, in *2017 2nd International Conference for Convergence in Technology, I2CT 2017*, pp. 1–6, doi: 10.1109/I2CT.2017.8226219, 2017.

[2] J. Brandt, R. Deters, G. Ananda, and M. Selig, Small-Scale Propeller Performance at Low Speeds – Online Database, http://www.ae.illinois.edu/m-selig/props/propDB.html (accessed May 01, 2018), 2010.

[3] A. Seeni, *Effect of Grooves on Aerodynamic Performance of a Low Reynolds Number Propeller*, PhD Thesis, Universiti Sains Malaysia, Penang, Malaysia, 2020.

[4] R. W. Deters, G. K. Ananda, and M. S. Selig, Reynolds Number Effects on the Performance of Small-Scale Propellers, in *32nd AIAA Applied Aerodynamics Conference*, no. June, pp. 1–43, doi: 10.2514/6.2014-2151, 2014.

[5] J. Brandt and M. Selig, Propeller Performance Data at Low Reynolds Numbers, in *49th AIAA Aerospace Sciences Meeting including the New Horizons Forum and Aerospace Exposition*, no. January, pp. 1–18, doi: 10.2514/6.2011-1255, 2011.

[6] A. M. Alakashi and I. B. Basuno, Comparison between Structured and Unstructured Grid Generation on Two Dimensional Flows Based on Finite Volume Method (FVM), *Int. J. Mining, Metall. Mech. Eng.*, vol. **2**, no. 2, pp. 97–103, 2014.

[7] B. E. Launder and D. B. Spalding, The numerical computation of turbulent flows, *Comput. Methods Appl. Mech. Eng.*, vol. **3**, no. 2, pp. 269–289, doi: 10.1016/0045-7825(74)90029-2, 1974.

[8] * * * ANSYS, *ANSYS FLUENT User's Guide*, no. January. ANSYS Inc., Canonsburg, PA, USA, p. 734, 2015, [Online]. Available: http://cdlab2.fluid.tuwien.ac.at/LEHRE/TURB/Fluent.Inc/v140/flu_ug.pdf.

[9] D. C. Wilcox, Formulation of the k-ω Turbulence Model Revisited, *AIAA J.*, vol. **46**, no. 11, pp. 2823–2838, doi: 10.2514/1.36541, 2008.

[10] F. Menter, *Zonal Two Equation k-ω Turbulence Models for Aerodynamic Flows*, 1993.

[11] * * * ANSYS Inc., ANSYS Fluent Theory Guide, Canonsburg, PA, USA, 2013.

[12] R. Deters, *Performance and Slipstream Characteristics of Small-Scale Propellers at Low Reynolds Numbers*, PhD Thesis, Department of Aerospace Engineering, University of Illinois at Urbana-Champaign, 2014.

[13] D. W. Zingg and P. Godin, A perspective on turbulence models for aerodynamic flows, *Int. J. Comut. Fluid Dyn.*, vol. 23, no. 4, pp. 327–335, doi: 10.1080/10618560902776802, 2009.

[14] W. J. Youden, Graphical Diagnosis of Interlaboratory Test Results, *J. Qual. Technol.*, vol. **4**, no. 1, pp. 29–33, doi: 10.1080/00224065.1972.11980509, Jan. 1972.

[15] M. Terziev, T. Tezdogan, and A. Incecik, Application of eddy-viscosity turbulence models to problems in ship hydrodynamics, *Ships Offshore Struct.*, pp. 1–24, doi: 10.1080/17445302.2019.1661625, Aug. 2019.